Insect Biochemistry and Molecular Biology 82 (2017) 52–61

Contents lists available at ScienceDirect

Insect Biochemistry and Molecular Biology

journal homepage: www.elsevier.com/locate/ibmb

Co-option of the sphingolipid metabolism for the production of nitroalkene defensive chemicals in termite soldiers

Anna Jirošová [a], Andrej Jančařík [a], Riya C. Menezes [b], Olga Bazalová [c], Klára Dolejšová [a, d], Heiko Vogel [b], Pavel Jedlička [a], Aleš Buček [a], Jana Brabcová [a], Pavel Majer [a], Robert Hanus [a, **], Aleš Svatoš [a, b, *]

[a] The Institute of Organic Chemistry and Biochemistry of the Czech Academy of Sciences, Flemingovo n. 2, 166 10 Prague, Czechia
[b] Max-Planck Institute for Chemical Ecology, Hans-Knöll-Str. 8, 07745 Jena, Germany
[c] Biology Centre CAS, Branišovská 31, CZ-37005 České Budějovice, Czechia
[d] Faculty of Science, Charles University in Prague, Viničná 7, 128 44 Prague, Czechia

ARTICLE INFO

Article history:
Received 23 November 2016
Received in revised form
20 January 2017
Accepted 20 January 2017
Available online 23 January 2017

Keywords:
Biosynthesis
Labeled probes
Chemical defense
Prorhinotermes simplex
Metabolomics
Transcriptomics

ABSTRACT

The aliphatic nitroalkene (*E*)-1-nitropentadec-1-ene (**NPD**), reported in early seventies in soldiers of the termite genus *Prorhinotermes*, was the first documented nitro compound produced by insects. Yet, its biosynthetic origin has long remained unknown. Here, we investigated in detail the biosynthesis of **NPD** in *P. simplex* soldiers. First, we track the dynamics in major metabolic pathways during soldier ontogeny, with emphasis on likely **NPD** precursors and intermediates. Second, we propose a hypothesis of **NPD** formation and verify its individual steps using *in vivo* incubations of putative precursors and intermediates. Third, we use a *de novo* assembled RNA-Seq profiles of workers and soldiers to identify putative enzymes underlying **NPD** formation. And fourth, we describe the caste- and age-specific expression dynamics of candidate initial genes of the proposed biosynthetic pathway.

Our observations provide a strong support to the following biosynthetic scenario of **NPD** formation, representing an analogy of the sphingolipid pathway starting with the condensation of tetradecanoic acid with L-serine and leading to the formation of a C_{16} sphinganine. The C_{16} sphinganine is then oxidized at the terminal carbon to give rise to 2-amino-3-hydroxyhexadecanoic acid, further oxidized to 2-amino-3-oxohexadecanoic acid. Subsequent decarboxylation yields 1-aminopentadecan-2-one, which then proceeds through six-electron oxidation of the amino moiety to give rise to 1-nitropentadecan-2-one. Keto group reduction and hydroxyl moiety elimination lead to **NPD**. The proposed biosynthetic sequence has been constructed from age-related quantitative dynamics of individual intermediates and confirmed by the detection of labeled products downstream of the administered labeled intermediates. Comparative RNA-Seq analyses followed by qRT-PCR validation identified orthologs of serine palmitoyltransferase and 3-ketodihydrosphingosine reductase genes as highly expressed in the **NPD** production site, i.e. the frontal gland of soldiers. A dramatic onset of expression of the two genes in the first days of soldier's life coincides with the start of **NPD** biosynthesis, giving further support to the proposed biosynthetic hypothesis.

1. Introduction

The occurrence of specialized defenders, the soldiers, has been among the crucial steps of social evolution in several groups of social insects, such as eusocial thrips, aphids, and termites (Crespi, 1994; Tian and Zhou, 2014). Beside mechanical defensive adaptations, the soldiers of many social insects evolved chemical weapons, very diversified in terms of both structural richness and the function of defensive chemicals. This is particularly true in termites. The soldiers of the advanced termite clade Neoisoptera (Engel et al., 2009) are equipped with a unique exocrine organ, the frontal gland, which secretes chemically diversified and often

* Corresponding author. Max-Planck Institute for Chemical Ecology, Hans-Knöll-Str. 8, 07745 Jena, Germany.
** Corresponding author.
E-mail addresses: robert@uochb.cas.cz (R. Hanus), svatos@ice.mpg.de (A. Svatoš).

http://dx.doi.org/10.1016/j.ibmb.2017.01.008
0965-1748/

Abbreviations

NPD	(*E*)-1-nitropentadec-1-ene
-1d; 0d; 1d; 3d; 7d; 12d; 18d; 25d; 30d+	soldier age category in days
D_{27}-**X**	particular compound labeled by 27 deuterium atoms in the hydrocarbon chain
[^{15}N,$^{13}C_3$]-**X**	particular compound labeled ^{15}N,$^{13}C_3$
[^{15}N]-**X**	particular compound labeled ^{15}N
DSR	3-ketodihydrosphingosine reductase
SPT	serine palmitoyltransferase
RP49	ribosomal protein 49
GSH	glutathione
FAS	fatty acid synthase
TAG	triacylglycerol
FAs	fatty acids
CYP	cytochrome P450
RNA-Seq	RNA sequencing
qRT-PCR	quantitative reverse transcription polymerase chain reaction
UPLC-ESI-MS/MS	ultra-performance liquid chromatography with electrospray ionization and tandem mass spectrometry
GC-MS	gas chromatography with mass spectrometric detection
PCA	principal component analysis

complex defensive blends, ranking the termites among the insect taxa with the richest chemical defenses (Prestwich, 1984).

Termite defensive chemistry includes a variety of chemical classes. Among these, *de novo* synthesized terpenoids, i.e. monoterpenes, sesquiterpenes and especially the complex and novel polycyclic diterpenes, are prominent (Šobotník et al., 2010). Aliphatic chains with electrophilic head groups, such as α,β-unsaturated carbonyls, represent another class of termite defensive chemicals, acting as electrophilic contact poisons (Spanton and Prestwich, 1981, 1982). Termites rarely synthesize nitrogen-containing defensive compounds, likely due to their predominant lignocellulose diet (Šobotník et al., 2010). As an exception, aminosaccharides and ceramides have been identified in soldiers of the genus *Coptotermes* (Rhinotermitidae) and, more importantly, nitroalkenes are known to be produced by soldiers of the tropical genus *Prorhinotermes* (Rhinotermitidae). Their frontal gland reservoirs contain up to 300 μg of (*E*)-1-nitropentadec-1-ene (referred to as **NPD** below), equivalent to over 10% of their body mass, together with a few minor nitroalkene, nitroalkane and nitrodiene homologs (Chuah et al., 1990; Piskorski et al., 2007; Vrkoč and Ubik, 1974). The electron-withdrawing potential of the **NPD** nitro group results in mutagenicity or acute toxicity of the compound due to alkylation of nucleic acids and proteins (Kuldová et al., 1999; Spanton and Prestwich, 1982).

The occurrence of nitro compounds in *Prorhinotermes* termites is puzzling since the nitro group formation is uncommon in the biosynthetic repertoire of insects and other arthropods (Parry et al., 2011); only a handful of cases have recorded the *de novo* synthesis of nitro compounds (Hall et al., 1992; Kuwahara et al., 2003; Meinwald et al., 1975; Sonenshine, 2006). Even though **NPD** was described in 1974 as the first insect-produced nitro compound (Vrkoč and Ubik, 1974), its biosynthetic origin has remained unknown. In our recent work, we hypothesized that **NPD** arises through a sphingolipid-like biosynthetic pathway starting with the condensation of the amino acids serine or glycine with tetradecanoic acid (Jirošová et al., 2014) and proposed two alternative scenarios leading to **NPD**.

In the present study, we verify our predictions on **NPD** biogenesis using metabolomic analyses, by tracking age-related dynamics in the occurrence of putative intermediates in young soldiers, and by incorporation experiments with newly synthesized deuterium-labeled intermediates. In addition, we target the genes coding for enzymes of the initial steps of **NPD** biosynthesis in the frontal glands of soldiers using *de novo* transcriptome assembly of tissue-specific RNA-Seq samples of soldiers and workers and qRT-PCR validation.

2. Material and methods

2.1. Termites

Colonies of *Prorhinotermes simplex* (Hagen) originated from Piñar del Rio, Cuba (1989), and Fort Lauderdale, Florida, USA (2003). Six mature colonies were transported to the laboratory in Prague, Czech Republic, held in large glass containers at 26 °C and elevated humidity, and fed with spruce wood blocks. The development of new soldiers was induced by removing all soldiers from the colonies. Within 6 weeks, new soldiers had developed in these colonies: workers became presoldiers, a transitional stage which lasted 13–17 days (Hanus et al., 2006). During the critical period, colonies were inspected daily, and desired developmental stages were removed and kept at 26 °C, with groups of workers allowed to develop in 9 cm Petri dishes, lined with moistened sand and provided with spruce blocks as food, until the required age. A presoldier approaching the molt to soldier can be recognized one day before the ecdysis because the dark mandibles of the future soldier are visible through the transparent presoldier cuticle.

For the incorporation studies, 4- to 5-day-old soldiers were used. For the metabolomic analyses, we used presoldiers in the middle of the presoldier stage (ps), presoldiers one day before ecdysis to soldiers (-1d), soldiers less than 24 h after eclosion (0d), and 1-, 3- and 7-day-old soldiers (1d, 3d, 7d). The analyses were performed with pooled extracts of five individuals of the given age category in three independent replicates. Total **NPD** production was tracked in soldiers up to 25 days after eclosion (12d, 18d, 25d) and in mature soldiers, older than 30 days (30d+), always using seven replicates (individual soldiers) per age category, using gas chromatography with flame-ionization detector. Intact mature workers from the same colonies were used as controls when appropriate.

2.2. Synthesis of intermediates and metabolites

The following standards of precursors and putative intermediates were synthesized: 1-nitropentadecan-2-one (**6**), 1-nitropentadecan-2-ol (**7**), 1-aminopentadecan-2-ol (**8**) and **NPD**. The following analogs labeled with deuterium at 13 carbon atoms of the aliphatic chain were synthesized: D_{27}-(2*S*,3*R*)-2-aminohexadecane-1,3-diol (D_{27}-**2**), D_{27}-(2*R*,3*R*)-2-amino-3-hydroxyhexadecanoic acid (D_{27}-**3**), D_{27}-1-nitropentadecan-2-ol (D_{27}-**7**), D_{27}-1-aminopentadecan-2-ol (D_{27}-**8**) and D_{27}-(*E*)-1-nitropentadec-1-ene (D_{27}-**NPD**). Full experimental details on the chemical synthesis are given in Jirošová et al. (in prep.). Synthesis of labeled and non-labeled **7**, D_{27}-**7**, **NPD**, and D_{27}-**NPD** was described previously (Jirošová et al., 2014). See Table 1 and Fig. 1 for structures and labeling.

2.3. In vivo incorporation studies

Labeled precursors of **NPD** biosynthesis were purchased from Sigma Aldrich. (^{15}N,$^{13}C_3$)-L-serine and (^{15}N)-glycine were diluted in sterilized water to 2.5 mg/ml. 10 μl of 1 M NaOH was added to

Table 1
MS characteristics of likely intermediates of the **NPD** biosynthetic pathway detected in soldier extracts.

Compound no	Chemical name	Retention time (min)	*m/z* $[M+H]^+$ or $[M + NH_4]^+$	δ (ppm)	Elemental composition
1	2-amino-1-hydroxyhexadecan-3-one	16.16	272.25816	−0.246	$C_{16}H_{34}O_2N$
2	2-aminohexadecane-1,3-diol	15.82	274.27359	−0.466	$C_{16}H_{36}O_2N$
3	2-amino-3-hydroxyhexadecanoic acid	16.11	288.25319	−0.452	$C_{16}H_{34}O_3N$
4	2-amino-3-oxohexadecanoic acid	16.13	286.23754	−0.13	$C_{16}H_{32}O_3N$
5	1-aminopentadecan-2-one	15.43	242.24776	−0.35	$C_{15}H_{32}ON$
6	1-nitropentadecan-2-one[a]	26.99, broad	289.24861	0.14	$C_{15}H_{33}O_3N_2$
8	1-aminopentadecan-2-ol	16.26	244.26341	−0.33	$C_{15}H_{34}ON$
NPD	(*E*)-1-nitropentadec-1-ene[a]	16.72	273.25331	−0.345	$C_{15}H_{33}O_2N_2$

[a] Detected as $[M + NH_4]^+$.

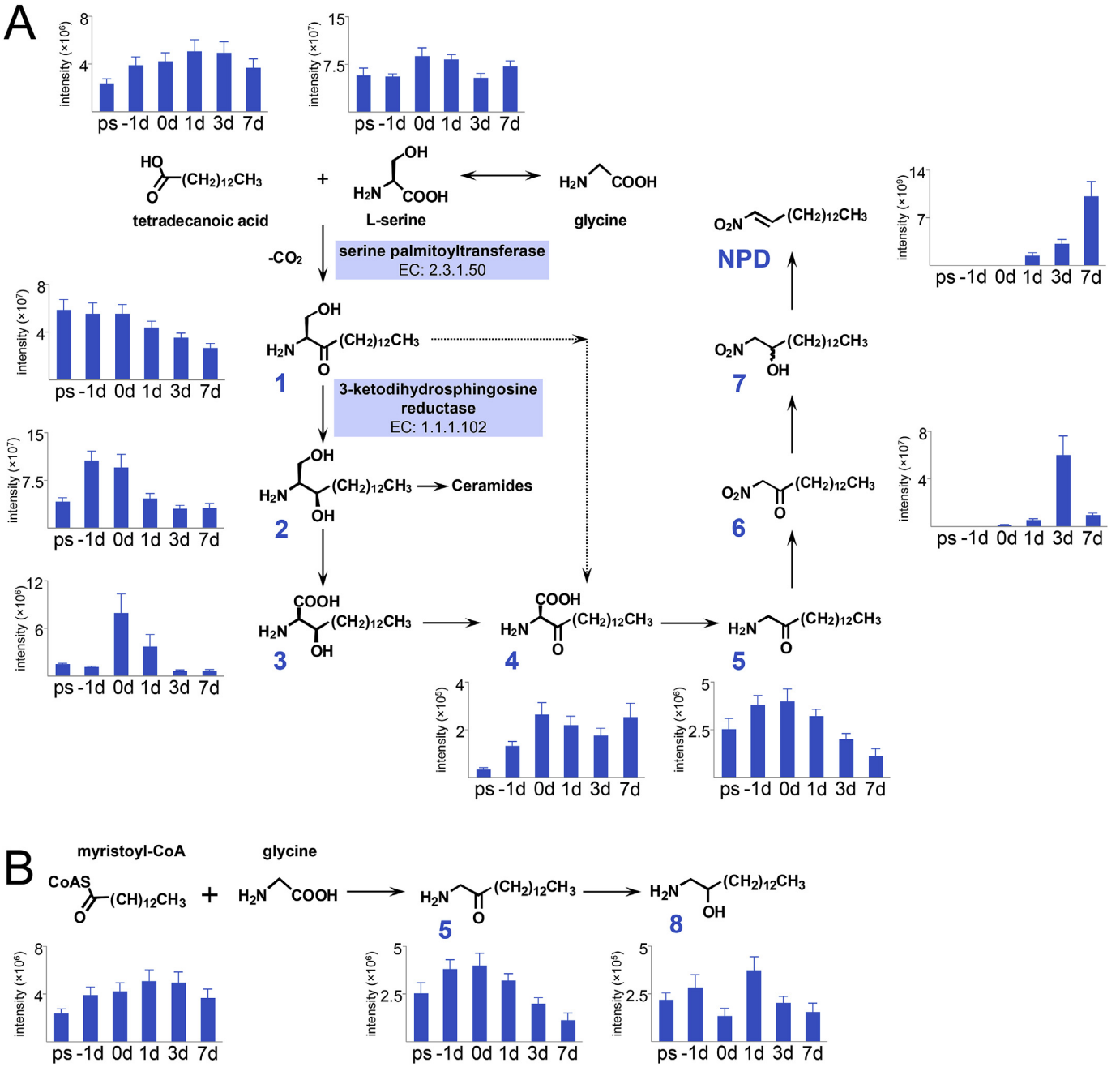

Fig. 1. Proposed biosynthesis of **NPD** in soldiers of *P. simplex* and age-related quantitative dynamics in the occurrence of individual precursors, intermediates and products, inferred from the metabolomic study. A. Main scenario (solid arrows) and an eventual alternative (dashed arrows). B. Proposed origin of the amino alcohol **8** identified in soldiers. Bars show the means, whiskers the standard errors of mean of detected intensities for three replicates from each caste or age category. ps, presoldier; -1d, pharate soldiers 1 day before ecdysis from presoldiers; 0–7d, soldier post-ecdysis age in days.

1.25 mg of (D_{27})-tetradecanoic acid or (1,2-$^{13}C_2$)-tetradecanoic acid and the obtained sodium salt was diluted by 10% aqueous solution of Tween 20 to 1 mg/ml. Polydeuterated standards of putative intermediates D_{27}-**2**, D_{27}-**3**, D_{27}-**8** and D_{27}-**NPD** were diluted in 10% aqueous solution of Tween 20 to 1 mg/ml (compounds D_{27}-**3**, D_{27}-**8** and D_{27}-**NPD**) or in sterilized water (compound D_{27}-**2**) to 1 mg/ml.

Solutions or emulsions of the precursors and intermediates were warmed to 40 °C and sonicated prior to injection. 0.25 μl of the solutions or emulsions was injected into the thorax of cold-anesthetized soldiers (5 min at 5 °C) by the hind leg articulation using a 5 μl Hamilton syringe with a custom Hamilton needle (34/17/pstN/tapN)S (Chromservis, Prague, Czech Republic). Injected soldiers were placed back to the Petri dishes with workers and sampled 3 h or 3 days after the administration of the injections.

2.4. Sample preparation

For UHPLC-ESI-MS/MS system (Q-Exactive, Thermo) analyses, soldiers and control workers were vortexed in dichloromethane:methanol (2:1, v/v) (5 individuals per sample in 250 μl) for 40 min at room temperature. After short sonication, the samples were filtered through extracted cotton wool in glass Pasteur pipettes and 10 μl was injected into UPLC. For GC-FID analyses, individual soldiers were homogenized in glass homogenizer containing 50 μl of dichloromethane and sonicated for 5 min. The liquid fraction was injected into a GC.

2.5. UHPLC-ESI-MS

Samples were analyzed on Ultimate 3000 series RSLC (Dionex, Sunnyvale, CA, USA) system coupled to a Q-Exactive Plus Hybrid Quadrupole-Orbitrap Mass Spectrometer (Thermo Fisher Scientific, Bremen, Germany) equipped with an ESI source. The separation was performed on Acclaim RSLC column (2.1 × 150 mm, C18, 2.2 μm particles with 120 Å pore diameter, Thermo Scientific) using water with 0.1% formic acid as solvent A and acetonitrile with 0.1% formic acid as solvent B at 300 $\mu l/min^{-1}$ flow rate. The gradient was as follows: 0–3 min, 0% B; 3–15 min, 60% B; 15–30 min, 100% B; 30–38 min, 100% B; 38–38.1 min, 0% B; 38.1–45 min, 0% B. Each sample run was separated with a short gradient wash run: 0–3 min, 0% B; 3–8 min, 60% B; 8–14 min, 100% B; 14–20 min, 100% B; 20–20.5 min, 0% B; 20.5–25 min, 0% B. The orbitrap mass analyzer was set to 140,000 mass resolutions at *m/z* 200 and operated in positive or negative ion mode. For tandem MS/MS, masses of interest were selected in a quadrupole using 1 Da selection window, and normalized fragmentation energy was set from 10 to 35 V. The instrument was calibrated using commercial CalMix (Thermo) prior to each sequence. Continuum spectral data of *m/z* 100–1500 mass span were collected and analyzed using Xcalibur v.3.0.63 software (Thermo Fisher Scientific).

2.6. Data analysis

Principal component analysis (PCA) was performed with MetaboAnalyst 3.0., a web-based tool for metabolomic data processing, statistical analysis, and functional interpretation (Xia et al., 2015). PCA was performed on the full-scan data of the samples. The raw spectra were first converted to mzXML format using the MS Convert feature of ProteoWizard 3.0.3750. Data processing was subsequently carried out with R Studio 0.96.316 using the Bioconductor XCMS package (Smith et al., 2006), which contains the algorithms for peak detection, peak deconvolution and peak alignment. The result – a compilation of mzmed, mzmin, mzmax, rtmed, rtmin, rtmax, and peak intensities values – was uploaded into Metaboanalyst as a peak intensity table. Data filtering was implemented by detecting noninformative variables that are characterized by near-constant values throughout the experimental conditions. Filtering was accomplished by comparing their robust estimate interquartile ranges (IQR). The data were then normalized to make individual features more comparable. Out of the 5339 features originally detected, 3203 were used for the PCA. PC1 accounted for 48% and PC2 accounted for 19% of the variance, respectively, and contributed to the best separation of the groups. Finally, a 2D score plot was constructed and 95% confidence regions for each group marked.

For semi-quantification based on the retention times and mass spectra of reference compounds, **NPD** and its precursors and likely intermediates were identified in termite extracts. Several primary metabolites involved in the Krebs cycle and metabolism of fatty acids (FAs) and amino acids were identified. The peaks of these compounds were integrated in Xcalibur and the area under the curve was calculated.

2.7. RNA-Seq and differential gene expression analysis

RNA was extracted from the following dissected tissues and body parts of *P. simplex* soldier and worker caste: 1) soldier abdominal cavity without gut and frontal gland (pooled tissue from 10 specimens); 2) soldier legs (10 specimens); 3) soldier frontal glands (50 specimens); 4) worker abdominal cavity without gut (10 specimens). Dissected tissues were stored in TRIzol (Invitrogen) at −80 °C prior to RNA extraction. Total RNA was extracted using standard phenol–chloroform procedure with TRIzol according to the manufacturer's protocol (Life Technologies), followed by digestion of DNA contaminants with TURBO DNase (Ambion) at 37 °C for 1h and subsequent RNA purification using the RNeasy Mini Kit (Qiagen) according to the manufacturer's protocol for RNA cleanup. The quantity of RNA was determined using a Nanodrop ND-1000 UV/Vis spectrophotometer (Thermo Fisher Scientific). The integrity of the RNA was verified using an Agilent 2100 Bioanalyzer and a RNA 6000 Nano Kit (Agilent Technologies, Palo Alto, CA).

Tissue-specific transcriptome sequencing of the four different RNA samples was performed with poly(A)+ enriched mRNA fragmented to an average of 150 nucleotides. Sequencing was carried out by the Max Planck Genome Center Cologne (MPGCC) on an Illumina HiSeq2500 Genome Analyzer platform using paired-end (2 × 100 bp) reads. This yielded approximately 25 million paired-end reads for each of the four samples. Quality control measures, including the filtering of high-quality reads based on the score given in fastq files, removal of reads containing primer/adaptor sequences and trimming of read length, were carried out using CLC Genomics Workbench v8.1 (http://www.clcbio.com). The *de novo* transcriptome assembly was carried out with the same software, combining all of the four RNA-Seq samples, and selecting the presumed optimal consensus transcriptome as described in Vogel et al. (2014). The resulting final *de novo* reference transcriptome assembly (backbone) of *P. simplex* contained 79,916 contigs (minimum contig size = 300 bp) with a N50 contig size of 1486 bp and a maximum contig length of 27,056 bp. The transcriptome was annotated using BLAST, Gene Ontology and InterProScan searches using BLAST2GO PRO v3.1 (www.blast2go.de).

Digital gene expression analysis was carried out using CLC Genomics Workbench v8.1 to generate BAM (mapping) files, and QSeq Software (DNAStar Inc., Madison, WI, USA) was then used to remap the Illumina reads from all four samples onto the reference transcriptome followed by counting the sequences to estimate expression levels, using previously described parameters for read mapping and normalization (Vogel et al., 2014).

2.8. RT-PCR

The alimentary canals of all investigated termites were removed to prevent contamination by symbiont RNA. Remaining bodies were immediately frozen in liquid nitrogen and stored at −80 °C. Total RNA was isolated using TRI Reagent® (Sigma Aldrich) following the manufacturer's protocol. RNA isolates were treated with RQ1 RNase-Free DNase (Promega) to eliminate contaminant DNA. The cDNA template was generated from 1.5 μg of the respective total RNA using the SuperScript III First-Strand Synthesis System (Invitrogen by Life Technologies) and random hexamers.

The partial mRNA sequences of both transcribed target genes as well as of the housekeeping genes, i.e. *3-ketodihydrosphingosine reductase* (EC 1.1.1.102, *DSR*), *serine palmitoyltransferase* (EC 2.3.1.50, *SPT*) and *ribosomal protein 49* (*RP49*), respectively; were adopted from annotated transcriptome. The sequences of specific primers used for amplification were as follows: *DSR*-F 5′ GTC CGC AGC TGT AAG AAG AAA AG 3′; *DSR*-R 5′ TCC TCC ACC TCA AGT ACA CAT AAA 3′; *SPT*-F 5′ TCC GGC AGA GAT TGA AA 3′; *SPT*-R 5′ TGC CGA AAG ACA GAA GC 3′; *RP49*-F 5′ CTG GTG CAT AAC GTG AAG GAA CT 3′; *RP49*-R 5′ CAG GCG AGC ATT AGC ATT TGT A 3′. The RT-PCR was performed using a LightCycler 480 qRT-PCR System (Roche) with SYBR green fluorescent labels and 200 nM of each primer. The PCR program setting was as follows: initial denaturation for 15 min at 95 °C, followed by 40 cycles of denaturation at 95 °C for 30 s and annealing/extension at 60 °C for 30 s. A final melting-curve step was included post-PCR (rising from 60 °C to 95 °C at 0.1 °C steps every 5 s) to confirm the absence of any non-specific amplification. The efficiency of each primer pair was assessed by constructing a standard curve through five serial dilutions. Each qRT-PCR experiment consisted of three independent biological replicates (two termites per replicate), with technical duplicates for each sample. The relative expression of both target genes was calculated using the method described by Pfaffl (2001).

3. Results

3.1. Identification of putative intermediates in P. simplex soldiers

In our previous work, we documented that serine, glycine and tetradecanoic acid are incorporated into **NPD** in *P. simplex* soldiers, and we proposed two alternative pathways of **NPD** formation starting from the C_{16}-ketosphinganine **1** (Jirošová et al., 2014). To verify either of the two biosynthetic alternatives and to understand individual steps of **NPD** biogenesis, we first performed a detailed search for previously proposed intermediates as well as for other likely metabolites and precursors of the biogenesis in 3d soldiers using UPLC-HRMS. The age-dependent quantification of **NPD** production in young soldiers suggested that the onset of biosynthetic activity was very early after the ecdysis of soldiers from the presoldier stage (Jirošová et al., in prep.). Therefore, we selected the 3d soldiers as an optimum age category in which most biosynthetic steps should be active.

Liquid chromatography using C18 column with acetonitrile/water elution solvent system and high resolving power and precision of Q-Exactive Plus orbitrap mass analyzer enabled us to separate all compounds of interest and assign the molecular composition to them. The minimum deviations of the calculated exact masses from the observed values (0.13–0.47 ppm) implicated only one molecular formula in the ±1 ppm window. Whenever synthetic standards, native or labeled, were available, tandem mass spectra were used to confirm the compound assignment (see Jirošová et al., in prep. for CID spectra and SIMs traces of identified compounds), which was further verified by the co-elution of standards with extracts. In 3d soldiers, we detected all (**1**–**6**) but one (**7**) intermediates of the principal biosynthetic cascade depicted in Fig. 1, including the final product, **NPD** (Table 1). In contrast, we did not detect any phosphorylated intermediates either in positive or in negative operation mode. This makes unlikely the previously proposed scenario of **NPD** formation via the phosphorylation of C_{16} sphinganic acid (Jirošová et al., 2014), while giving support to our main hypothesis (Fig. 1A). In addition to the expected intermediates suggested in our hypothesized biosynthetic pathway, we also detected the amino alcohol **8**. This compound is likely formed from the direct condensation of tetradecanoic acid with glycine yielding aminoketone **5** that is subsequently reduced (see Fig. 1B). The enzymatic apparatus for this transformation is so far unknown; however, the analogous condensation of glycine with levulinic acid is described in the KEGG database, and the transcript for 5-aminolevulinate synthase [EC 2.3.1.37] is upregulated in the frontal gland (Fig. 4C). The alternative enzymatic condensation of glycine with acetyl-CoA catalyzed by 2-amino-3-ketobutyrate CoA ligase did not show the expected pattern (Fig. 4C).

3.2. Ontogenetic metabolomics

In the next step, we tracked the age-related dynamics in the quantitative patterns of the putative intermediates so as to validate the proposed biosynthetic cascade. In addition, we also focused the quantitative shifts in selected metabolites of fatty acids and in amino acid biosynthetic pathways and energy metabolism, with the aim of depicting a broader view of the metabolic transitions along the development of workers lacking the frontal gland and nitroalkenes, through the transitional stage of presoldiers, into the soldier stage, in which large amounts of nitrogen-rich defensive chemicals are produced. The dynamic changes in the metabolites **1**–**6** showed the trends (Fig. 1A) predicted from the early onset of **NPD** production immediately after the soldier eclosion (Jirošová et al., in prep.). **NPD** itself occurred in detectable quantities in the 1d soldiers and increased up to the 7d soldiers, the latest sampling point. The basic precursors, tetradecanoic acid and L-serine appeared to be constitutively available in all stages and age classes and were converted during the presoldier stage and later into the ketosphinganine **1**, showing a gradual depletion from 0d. The direct downstream product sphinganine **2** shows a rapid increase and a peak in -1d soldiers, followed by a slow decrease as it is converted into sphinganic acid **3**, which was found to be the most abundant in 0d soldiers. The two downstream intermediates **4** and **5** also show a maximum in 0d soldiers, followed by a gradual decrease of **5** seemingly through the transformation into nitroketone **6**, which occurs in detectable amounts as late as at 0d and peaks at 3d. Then it declines and is presumably fully channeled into **NPD**, showing a rapid increase from 3d to 7d.

The patterns of global metabolism revealed a small, yet distinguishable, transition from presoldier to the pharate − 1d and freshly molted 0d soldiers − followed by a dramatic stepwise shift during the first days after eclosion along the maturation of the soldier from 1d through 3d to 7d soldiers (Fig. 2). The quantitative patterns of major metabolites related to amino acid metabolism, fatty acid metabolism, antioxidative mechanisms, glycolysis, Krebs cycle, and metabolism of vitamins and cofactors are reported in Jirošová et al. (in prep).

Intensities of protonated amino acids are constant over all analyzed stages or gradually increase (Jirošová et al., in prep.). An important increase from very low values to a maximum at 7d was observed for aspartate and a dramatic stepwise increase from zero in presoldiers to a maximum at 1d, followed by an abrupt drop down to depletion in 7d soldiers was found for cysteine.

Interesting patterns were observed for the metabolites of

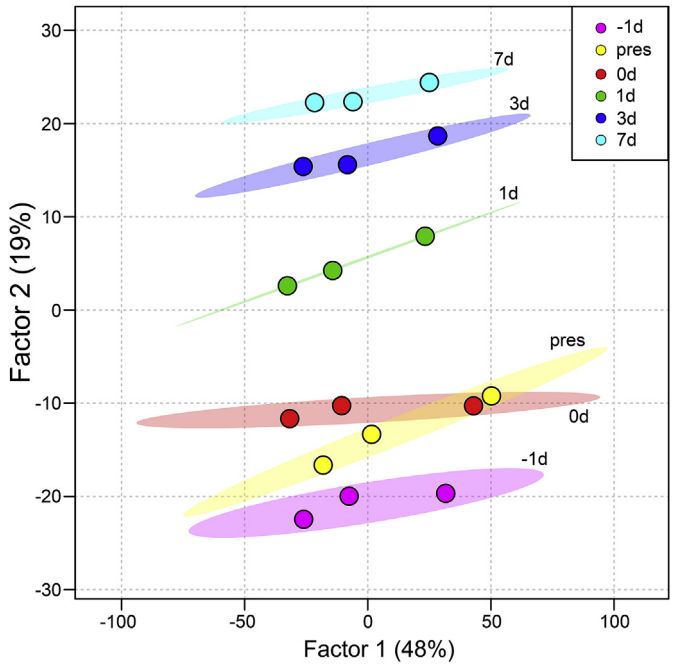

Fig. 2. Age-related dynamics in quantitative patterns of global metabolism analyzed in whole body extracts of presoldiers and early stages of soldier development. The graph represents the factor scores of the first two principal components of a PCA analysis calculated from normalized quantities of 3203 consistently detected metabolites. Ellipsoids mark 95% confidence regions for each considered group. ps, presoldier; -1d, pharate soldiers 1 day before ecdysis from presoldiers; 0–7d, soldier post-ecdysis age in days.

antioxidative pathways (Jirošová et al., in prep.). An initial increase in the quantities of glutathione (GSH) from the presoldier stage to -1d and 0d soldiers is followed by a drop down to zero in all older soldiers. Two putative GSH synthetase genes (*ProRhino_C15568* and *ProRhino_C19311*) are upregulated in the frontal gland (Fig. 4E). By contrast, an inverse metabolomics pattern was found for the **NPD**-GSH adduct, first occurring in 0d soldiers and soon reaching its maxima in 1d, 3d and 7d soldiers. An analogous pattern with a maximum in 1d soldiers was observed for the **NPD**-cysteine adduct. The formation of adducts is likely spontaneous, as gene(s) with a putative GSH transferase activity were not found.

While most of the fatty acids (Jirošová et al., in prep.) showed a stable pattern or a slow gradual increase over the studied time, the dynamic changes observed for hexadecanoic acid and hexadecenoic acid revealed a more complex variation. The former rises at a maximum at -1d and then dramatically decreases at 0d to accumulate at another maximum at 3d and fall down again at 7d. The latter shows a similarly complex trend with a local minimum at -1d and virtually complete depletion in 3d soldiers. This contrasts with the pattern of the C_{18} homologs, showing a stepwise increase until 3d. The intense upregulation of fatty acid synthases (FAS, Fig. 4D), predominantly in the abdominal cavity of soldiers, corresponds to metabolomics data and the limited supply of myristic acid stored in the fat body. We were not able to discern the substrate specificity of individual FAS transcripts, but FAS *ProRhino_C54,* for example, is strongly upregulated in the frontal gland tissue. Interestingly, FAS might bear C_{14}-like substrate specificity at the appropriate ionic strength in cells as shown in *D. melanogaster* (Derenobales and Blomquist, 1984).

3.3. In vivo incorporation of labeled amino acid and fatty acid precursors

The 140,000 mass resolution setting enabled an effective separation of mass signals of the $^{15}N_1$-containing isotopologs from the slightly heavier $^{13}C_1$ isotopologs, despite the difference of only 6.3 mDa. However, due to the low natural abundance of the ^{15}N isotope (0.36%) and the relatively low incorporation of the labeled substrates, reliable incorporation rates were available only for certain quantitatively major compounds of the pathway (Table 2). Very early after [^{15}N]-glycine injection into soldiers, a rapid onset of ^{15}N incorporation was observed for sphinganine **2** (with determined incorporation rate 15.35), and relatively less incorporation into its precursor **1** and downstream products **5**, **8**, and **NPD**. ^{15}N incorporation into **NPD** (1.36) after only 3 h of incubation documents the rapid conversion of intermediates into the terminal product. At extended incubation times, the arising labeled products were substantially diluted by newly produced non-labeled products and thus the incorporation rates decreased (Table 2).

When labeled serine was injected, only triple-labeled [^{15}N,$^{13}C_2$]-**1** and [^{15}N,$^{13}C_2$]-**2** were detected after 3h, at 0.53 and 5.59 incorporation rate, respectively, together with the double-labeled [^{15}N,^{13}C]-**NPD**, showing 0.68 incorporation rate (Table 2). The absence of the corresponding isotopologs of the treatment of 3d soldier may be attributed to the dilution of the label by gradually increasing quantities of non-labeled compounds. Additionally, an isotopic effect should be considered for serine when compared with glycine, as the original condensation product with tetradecanoic acid survives a decarboxylation step when $^{13}CO_2$ is liberated. Finally, [$^{13}C_2$]-tetradecanoic acid was injected, but the $^{13}C_2$ isotope mass peak intensities were indistinguishable from natural isotopic distributions.

3.4. Chemical synthesis of labeled intermediates

Encouraging results obtained with labeled amino acids, confirming the incorporation of these precursors into the putative intermediates and final product, prompted us to prepare a series of D_{27}-labeled **NPD** precursors. The enantioselective synthesis of D_{27}-**2** and D_{27}-**3** was performed by the addition of D_{27}-myristaldehyde to the Schiff's base formed by camphor and glycine ethyl ester. The resulting adduct had 2*R*, 3*R*-erythro configuration corresponding to naturally occurring cell membrane lipid sphinganines. Acidic hydrolysis of this adduct provided ethyl-D_{27}-2-amino-3-hydroxyhexadecanoate, which was purified by column chromatography and either hydrolyzed to acid D_{27}-**3** or reduced to D_{27}-**2**. D_{27}-**8** was prepared from (D_{27})-tetradecanoic acid, which was first converted to the corresponding aldehyde and then condensed with nitromethane to D_{27}-**7**. This nitro alcohol was then reduced to D_{27}-**8** by catalytic hydrogenation. See Jirošová et al. (in prep.) for details on the synthesis.

3.5. In vivo incorporation of deuterium labeled precursors and intermediates

The deuterium-labeled precursors and intermediates (D_{27})-tetradecanoic acid, D_{27}-**2**, and D_{27}-**3**, were used for 3 h and 3 days incubations in living soldiers. After 3h of incubation, we were able to detect the incorporation of the labeled compounds into the immediate downstream products of the biosynthetic pathway, i.e. into D_{27}-**1**, D_{27}-**2**, and D_{27}-**3** in the case of (D_{27})-tetradecanoic acid administration and into D_{27}-**3** in the case of D_{27}-**2** administration. In addition, we detected the incorporation into the final **NPD** for all three injected compounds (Table 3). In the datasets for the 3d soldiers the incorporation into downstream intermediates was

Table 2
Incorporation rates of labeled amino acids into likely intermediates of the **NPD** biosynthetic pathway after 3 h and 3 days of *in vivo* incubation in 4- to 5-day-old soldiers.

Incubation time	Injected precursor	Incorporation rate (100 × labeled/native compound)					
		(^{15}N)-**1** (^{15}N,$^{13}C_2$)-**1**	(^{15}N)-**2** (^{15}N,$^{13}C_2$)-**2**	(^{15}N)-**5** (^{15}N,^{13}C)-**5**	(^{15}N)-**6** (^{15}N,^{13}C)-**6**	(^{15}N)-**8** (^{15}N,^{13}C)-**8**	(^{15}N)-**NPD** (^{15}N,^{13}C)-**NPD**
3 days	(^{15}N)-glycine	1.59	15.35	2.68		2.73	1.36
	(^{15}N,$^{13}C_3$)-serine	0.53	5.59				0.68
3 h	(^{15}N)-glycine	0.40	0.45	2.02	0.29		0.38
	(^{15}N,$^{13}C_3$)-serine						0.51

Table 3
Incorporation rates of deuterium-labeled precursors and intermediates into likely intermediates of **NPD** biosynthetic pathway after 3 h and 3 days of *in vivo* incubation in 4- to 5-day-old soldiers.

Incubation time	Injected precursor	Incorporation rate (100 × labeled/native compound)			
		D_{27}-**1**	D_{27}-**2**	D_{27}-**3**	D_{27}-**NPD**
3 h	(D_{27})-tetradecanoic acid	*trace*	34	4	0.045
	D_{27}-**2**	–	1973	25	0.007
	D_{27}-**3**	–	–	87949	*trace*
	signal intensity of native intermediate	5×10^7	2×10^8	7×10^6	2×10^{10}
3 days	(D_{27})-tetradecanoic acid	–	2.98	–	0.151
	D_{27}-**2**	–	34	–	0.16
	D_{27}-**3**	–	–	9000	–
	signal intensity of native intermediate	6×10^7	1×10^8	6×10^6	4×10^{10}

detected only as D_{27}-**2** when (D_{27})-tetradecanoic acid was injected. By contrast, the labeling was clearly visible in **NPD** and was higher than at the 3h data point in the case of D_{27}-**2** and (D_{27})-tetradecanoic acid administration. The indiscernibility of some of the downstream intermediates could be related to limited sensitivity; in some cases, the intensity of the native intermediate was only 10^6 or less, and since the degree of label incorporation is low, the ions become indistinguishable from noise. The minimum reliable readout on the used instrument is ca 10^3 ion counts. Additionally, substantial secondary isotopic effect, due to presence of 27 deuterium atoms in labeled compounds, plays a role.

3.6. RNA-Seq

To enable identification of candidate genes of the **NPD** biosynthetic pathway and other genes related to soldier frontal gland-specific processes, we performed NextGen sequencing (RNA-Seq) using Illumina HiSeq technology with paired-end (2 × 100 bp) reads with RNA isolated from *P. simplex* soldier abdominal cavity without gut and frontal gland, soldier legs, soldier frontal glands and worker abdominal cavity without gut. We designed the RNA-Seq analysis based on the hypothesis that soldiers should express soldier-specific genes, *e.g.* related to frontal gland defense chemistry, and compared them with their abdominal cavity and legs (as reference tissues). In addition, we compared the data with the abdominal cavity of workers to elucidate caste differentiation. We combined these tissue and caste-specific datasets to build the *P. simplex de novo* transcriptome assembly (TA) and profiled the expression of candidate genes by aligning the Illumina 100-base pair sequence tags of each of the tissue samples with the TA-contig sequences. Based on the RNA-Seq mapping results, we first focused on genes associated with enzymes related to the observed metabolites (see 3.1–3.5), such as the nitrogen fixation and sphingolipid pathways (Fig. 4). As shown in Fig. 4C, the genes coding for two enzymes likely catalyzing the first two steps of the proposed NPD biogenesis, *i.e.* serine palmitoyltransferase (*SPT*, *ProRhino_C1378*) and 3-ketodihydrosphingosine reductase (*DSR*, *ProRhino_C2748*) are listed among the genes with the highest transcript levels in the frontal glands of soldiers. Next, we identified genes associated with other functional categories such as CYP, fatty acid biosynthesis pathways as well as genes which displayed soldier frontal gland-specific expression patterns and visualized these expression patterns across the four termite samples (Jirošová et al., in prep.). The genes most highly expressed in soldier frontal glands include a number of CYP enzymes, fatty acid biosynthesis-related enzymes and (among others) enzymes of the insect isoprenoid biosynthetic pathway (FPPS, GPPS) (Jirošová et al., in prep.).

3.7. Expression patterns of serine palmitoyltransferase and 3-ketodihydrosphingosine reductase

As shown in Fig. 3, the expression of both *SPT* and *DSR* dramatically increases in early days after soldiers develop from presoldiers, while being relatively very low in presoldiers and workers. Whereas *SPT* expression shows a slow stepwise growth with an onset in -1d soldiers and a peak at 3d, the abundance of *DSR* transcripts displayed an abrupt increase at -1d, contrasting with very low levels in presoldiers.

4. Discussion

In the present study, we characterized the biosynthetic pathways of the unique nitroalkene (*E*)-1-nitropentadec-1-ene (**NPD**) produced in large quantities as the main component of the defensive secretion of the frontal glands of soldiers in the termite genus *Prorhinotermes*. In our previous work, we postulated two alternative scenarios of **NPD** biogenesis, both starting as a modification of the sphingolipid pathway, constitutively present in organisms as a source of vital ceramides (Jirošová et al., 2014). Here, we provide multiple supporting evidence for one of these alternative pathways, and identify the intermediates of **NPD** biosynthesis along with age-related dynamics in **NPD** biogenesis using a combination of *in vivo* incubations of *de novo* synthesized labeled precursors and intermediates and mass spectrometric metabolomics. We also identify the orthologs of two enzymes catalyzing two initial steps of **NPD** biosynthetic pathway, i.e. the condensation of tetradecanoic acid with serine and the subsequent formation of **1** by means of RNA-Seq and qPCR validation.

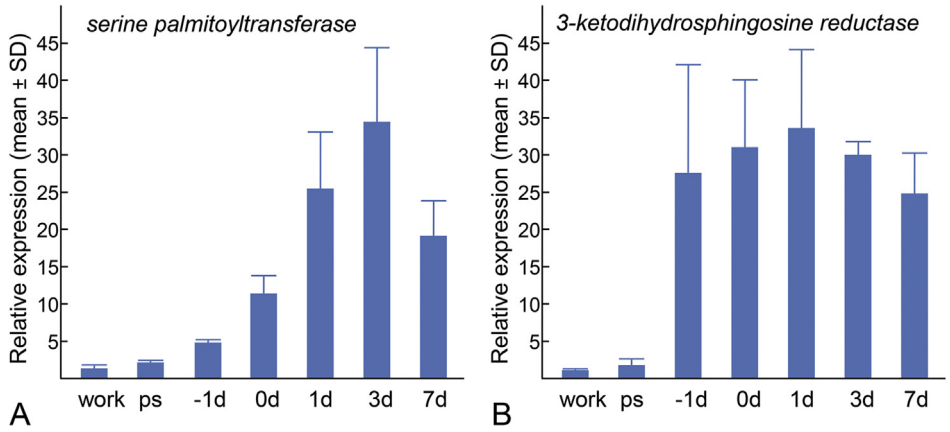

Fig. 3. Time dynamics in expression of *serine palmitoyltransferase* (*SPT*) and *3-ketodihydrosphingosine reductase* (*DSR*) in workers, presoldiers and early stages of soldier development. Bars show the means, whiskers the standard deviations for three replicates for each caste or age category. work, worker; ps, presoldier; -1d, pharate soldiers 1 day before ecdysis from presoldiers; 0–7d, soldier post-ecdysis age in days.

Our results indicate that the first of the previously proposed pathways proceeding from the C_{16} sphinganine through oxidation at the terminal hydroxyl to sphinganic acid and a series of intermediates activated by phosphorylation (Jirošová et al., 2014) is unlikely, because none of the putative phosphorylated intermediates was detected. By contrast, we unambiguously and consistently detected only the sphinganic acid (**3**) and a series of other non-phosphorylated likely intermediates, leading us to formulate the following biosynthetic route (Fig. 1): The first step is the condensation of serine with tetradecanoyl-CoA catalyzed by serine palmitoyltransferase (EC 2.3.1.50), identified as highly expressed transcripts in the soldier frontal gland and also partially in abdominal cavity. Five coding contigs showing the described patterns were identified (Fig. 4C). This enzymatic transformation provides ketosphinganine (**1**) after the elimination of carbon dioxide. Both serine and glycine ^{13}C and ^{15}N labeled were shown to be incorporated in **1**; however, deuterated **1** was not detected after injection of D_{27}-tetradecanoic acid, probably due to the fast turnover and dilution of the label by native compound. The level of **1**, which was higher even in presoldiers, gradually decreased in 1d soldiers. This condensation is common in many species and was extensively studied in *Drosophila melanogaster*; there, C_{14}-sphinganine and C_{16}-sphinganine are biosynthesized by the condensation of L-serine with dodecanoic or tetradecanoic acid, respectively (Fyrst et al., 2004). This step is catalyzed by the analog of the serine palmitoyl transferase PLP-dependent enzyme (Hanada, 2003), but in the case of *Drosophila,* it is preferably specific for shorter (C_{12}, C_{14}) fatty acid substrates (Adachi-Yamada et al., 1999).

The second step is the reduction of ketosphinganine C3-keto group into the sphinganine (**2**) C3-hydroxy group. Highly abundant transcripts of 3-ketodihydrosphingosine reductase (EC 1.1.1.105), an NADPH requiring dehydrogenase (Gault et al., 2010), were observed in transcriptome analysis (Fig. 4, Jirošová et al., in prep.). Mass spectral analysis indicated the highest isotopic label incorporation (5.59) of ^{15}N and ^{13}C originating from serine. An even higher incorporation rate (15.35 of ^{15}N) was observed after the injections of labeled glycine. The enzymatically catalyzed conversion of glycine to serine is highly likely to operate in termites as this transformation is a part of the amino acid interconversion pathway. Three corresponding contigs were established in the transcriptome (Fig. 4B), with one (*ProRhino_C10997*, serine mitochondrial isoform 1) showing high abundance in the frontal gland. The high label incorporation likely indicates that **2** accumulates in soldier body and is later channeled to **NPD** and/or ceramides. Ontogenetic metabolomics data showed a high level of **2** in -1d soldiers with gradual decrease along the maturation of the soldier. In contrast, the amounts of **NPD** increased at later stages. When isotopically labeled D_{27}-**2** was injected into 3d soldiers, labeled **NPD** was detected at low levels after 3 h of incubation (0.007 incorporation rate), and higher intensities after 3 days (0.16). Therefore, **2** appears to be one of the key intermediates in the **NPD** biosynthetic pathway.

Other parts of the biosynthetic scenario remain more elusive. We were not able to find the transcripts of the enzymes likely responsible for the proposed enzymatic transformations of **2** to sphinganic acid **4** and later to **NPD**. The acid **4** could hypothetically be formed by the two-step oxidation of sphinganine to acid **3** and **4**. Alternatively, **1** could be oxidized to **4** directly. Taking into account the metabolomic and incubation data, the more complex conversion of **2** to **4** via **3** is more likely. The rapid onset of **3** at 0d takes place one stage later than the onset of sphinganine **2** at -1d. Additionally, D_{27}-**2** was built into **3** with a high degree of incorporation. Regrettably, the low-signal intensity ($<10^6$) of non-labeled ketoacid **4** prevented us from observing the incorporation of deuterium into **4**. We have identified a number of CYP related transcripts with high transcript levels in the frontal gland (Jirošová et al., in prep.), but we cannot predict which of the corresponding enzymes is responsible for this oxidation step.

Acid **4** is decarboxylated to aminoketone **5**. This reaction is analogous to the enzymatic oxidative pyruvate-dependent amino acid decarboxylation sequence (Li et al., 2012). This reaction is responsible for the formation of important biogenic amines, such as histamine or GABA. However, **5** could be formed more directly from the condensation of glycine with tetradecanoic acid (Fig. 1B). This reaction is analogous to the formation of **1** by serine palmitoyltransferase, and the corresponding gene was localized in the transcriptome (Fig. 4C, *ProRhino_C2276*). A high ^{15}N nitrogen incorporation rate was observed (2.68 and 2.02 at 3 h and 3 days of incubation, respectively; Table 2). Whether this or another enzyme is responsible for this condensation remains to be established by the heterologous expression of the gene in cells and incubations with substrates.

The glycine-tetradecanoic acid pathway (Fig. 1B) may appear as a more parsimonious scenario; yet, it is difficult to verify experimentally and establish which of the two alternatives contributes more to **NPD** biosynthesis. Eventual blocking of either pathway is supposed to bring along an increased mortality through disruption of ceramide biosynthesis. To obtain more data on aminoketone **5** downstream metabolic transformations, we tried to prepare D_{27}-**5**; however, due to its instability we were not able to obtain it in

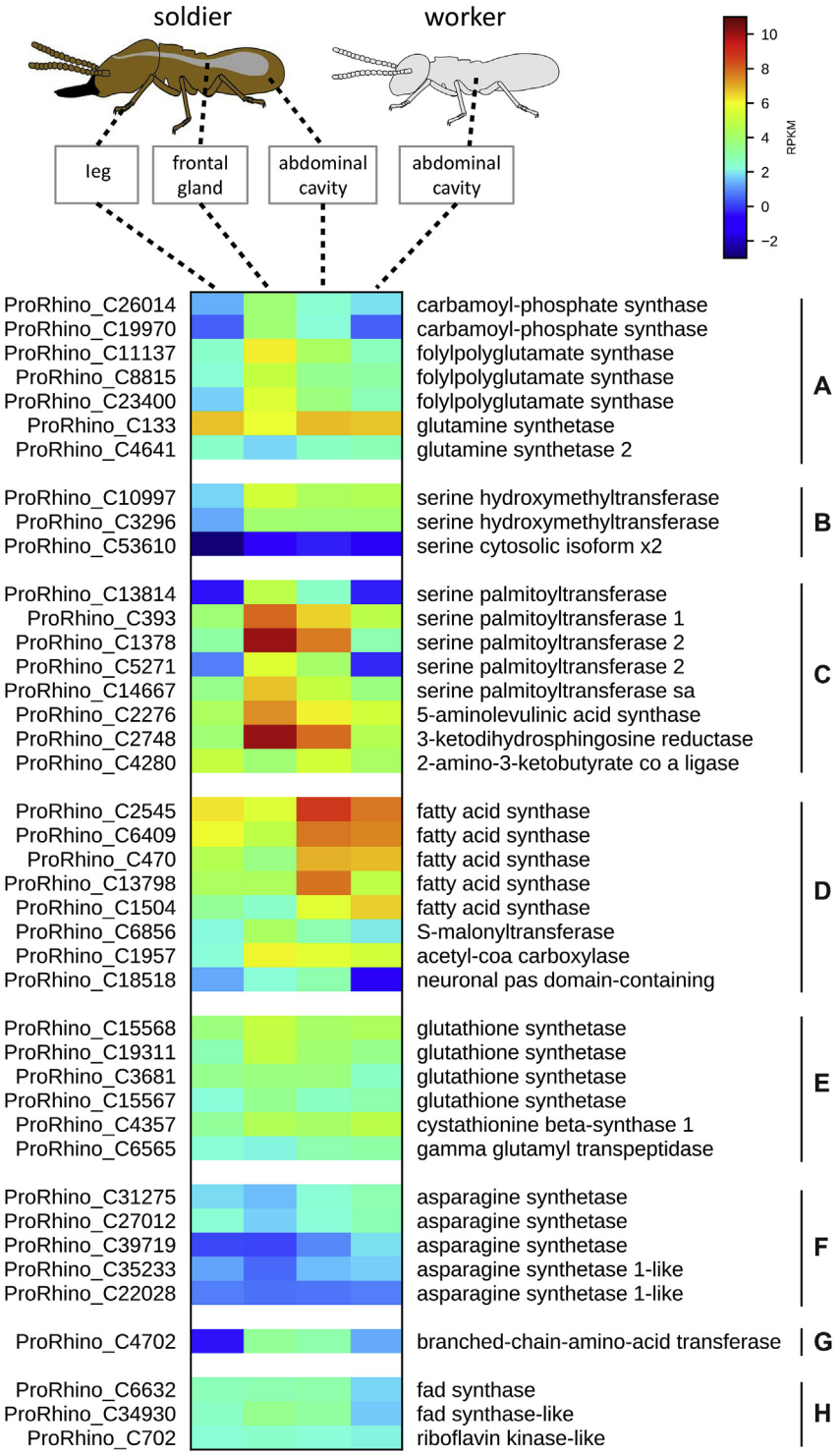

Fig. 4. Gene expression levels in three *P. simplex* tissues from soldiers (leg, frontal gland and abdominal cavity) and in control *P. simplex* workers. The mRNA levels, as represented by $\log_2$RPKM values, are shown in the gradient heat map from blue (−2) to red (10). Metabolic genes of interest corresponding to the metabolomic profiling are grouped according to their functions as glutamate (A), serine (B), serine and glycine condensation with CoA esters and reduction of ketogroup in sphinganine pathway (C), fatty acid (D), glutathione (E), asparagine (F), branched amino acids (G), and FAD (H) metabolism. (For interpretation of the references to colour in this figure legend, the reader is referred to the web version of this article.)

sufficient amounts and at a desired level of purity. From the large amounts of **NPD** produced, it is likely that soldiers are using both pathways. Aminoalcohol **8** detected in the extracts could be formed by the keto-group reduction analogous to **1**–**2** transformation. Its function in **NPD** biosynthesis has not been established, but similar compounds were shown to be strong inhibitors of ceramide synthesis, or part of toxic products made by fungi (see review by Pruett et al., 2008; Merrill, 2011). Thus, soldiers could eventually use **8** to increase the pool of sphinganine **1** for **NPD** production by blocking its downstream processing.

Both branches of **NPD** biosynthesis use tetradecanoic acid as a key substrate. The quantity of **NPD** in the adult *P. simplex* soldiers is about 300 μg per soldier, while the fat body contains only 30 μg TAGs per individual, and that represents about 0.8% of fresh body weight (3.6 mg on average; n = 10) (Šobotník et al., 2006). The most abundant FAs found in *P. simplex* soldiers TAGs are of 18 and 16 carbons. The content of TAGs with C_{14} acid, the precursor of the **NPD**, is less than 1% of the TAG relative concentration. When we compare C_{16} and C_{18} FAs amount to that of tetradecanoic acid (less than 0.03 μg/individual), it is unlikely that the fat body can be the storage site of tetradecanoic acid; thus the *de novo* biosynthetic origin of the tetradecanoic acid for the **NPD** is probable. The *de novo* biosynthesis hypothesis is further supported by metabolomics data on glycolysis and the Krebs cycle (see above). Additionally, transcriptomic data point to *de novo* fatty acid synthesis in the frontal gland and also in the abdominal cavity (Jirošová et al., in prep.), manifested by the upregulation of numerous FAS genes. FAS typically provide palmitate as the end product, but myristate may also be produced.

The crucial late step of **NPD** biosynthesis represents a sequence of the oxidation of the amino group in **5** via hydroxyl amine, oxime/nitroso intermediate to nitro group. This six-electron reaction is likely to be catalyzed by as yet unknown *N*-oxygenases. Even though we have identified putative intermediates of this oxidative sequence (data not shown) and a series of oxidases specifically expressed in the frontal glands of soldiers, our current state of knowledge does not allow for rigorous confirmation of the oxidation step. At the same time, it is likely that microbial genes are eventually involved in the oxidation. Only with a few exceptions (3-nitropropionate in plants or alkaloid nitropolyzonamine in the millipede *Polyzonium rosalbum*), the naturally occurring nitro compounds are produced by bacteria or fungi. As termites largely recruit microsymbionts, including bacteria, for wood degradation, nitrogen fixation and recycling (Bignell, 2011), the microbiota may also be involved in the production of nitro compounds. In brief, the oxidative conversion of the amino to nitro moiety during **NPD** biosynthesis remains an appealing topic for future studies.

Employing metabolomics, transcriptomics, and incubations of soldiers with labeled metabolic probes, we argue strongly that the sphinganine biosynthetic pathway is needed for the formation of crucial building blocks for **NPD** biosynthesis. Several downstream biosynthetic steps will be the subject of further investigation using more advanced metabolic profiling and by blocking critical points of the proposed **NPD** biosynthesis.

Acknowledgments

We are grateful to the Czech Science Foundation (project No: 13-25137P) and the Institute of Organic Chemistry and Biochemistry of the Czech Academy of Sciences (RVO: 61388963) for financial support and to Max Planck Society for instrumental and technical support. We thank David Doležel (Biology Center, CAS, Czech Republic) for valuable advices, and Emily Wheeler for editorial assistance.

References

Adachi-Yamada, T., Gotoh, T., Sugimura, I., Tateno, M., Nishida, Y., Onuki, T., Date, H., 1999. De novo synthesis of sphingolipids is required for cell survival by down-regulating c-Jun N-terminal kinase in *Drosophila* imaginal discs. Mol. Cell. Biol. 19, 7276–7286.

Bignell, D.E., 2011. Morphology, physiology, biochemistry and functional design of the termite gut: an evolutionary wonderland. In: Bignell, D.E., Roisin, Y., Lo, N. (Eds.), Biology of Termites: A Modern Synthesis. Springer, Dordrecht, pp. 375–412.

Chuah, C.H., Goh, S.H., Tho, Y.P., 1990. Chemical defense secretions of some species of Malaysian Rhinotermitidae (Isoptera, Rhinotermitidae). J. Chem. Ecol. 16, 685–692.

Crespi, B.J., 1994. Three conditions for the evolution of eusociality: are they sufficient? Insectes Soc. 41, 395–400.

Derenobales, M., Blomquist, G.J., 1984. Biosynthesis of medium chain fatty-acids in *Drosophila melanogaster*. Arch. Biochem. Biophys. 228, 407–414.

Engel, M.S., Grimaldi, D.A., Krishna, K., 2009. Termites (Isoptera): their phylogeny, classification, and rise to ecological dominance. Am. Mus. Novit. 1–27.

Fyrst, H., Herr, D.R., Harris, G.L., Saba, J.D., 2004. Characterization of free endogenous C-14 and C-16 sphingoid bases from *Drosophila melanogaster*. J. Lipid Res. 45, 54–62.

Gault, C.R., Obeid, L.M., Hannun, Y.A., 2010. An overview of sphingolipid metabolism: from synthesis to breakdown. In: Chalfant, C., DelPoeta, M. (Eds.), Sphingolipids as Signaling and Regulatory Molecules. Springer, New York, pp. 1–23.

Hall, D.R., Beevor, P.S., Campion, D.G., Chamberlain, D.J., Cork, A., White, R.D., Almestar, A., Henneberry, T.J., 1992. Nitrate esters: novel sex pheromone components of the cotton leafperforator, *Bucculatrix thurberiella* busck. (Lepidoptera, Lyonetiidae). Tetrahedron Lett. 33, 4811–4814.

Hanada, K., 2003. Serine palmitoyltransferase, a key enzyme of sphingolipid metabolism. BBA-Mol. Cell. Biol. L 1632, 16–30.

Hanus, R., Šobotník, J., Valterová, I., Lukáš, J., 2006. The ontogeny of soldiers in *Prorhinotermes simplex* (Isoptera, Rhinotermitidae). Insectes Soc. 53, 249–257.

Jirošová, A., Majer, P., Jančařík, A., Dolejšová, K., Tykva, R., Šobotnik, J., Jiroš, P., Hanus, R., 2014. Sphinganine-like biogenesis of (*E*)-1-nitropentadec-1-ene in termite soldiers of the genus *Prorhinotermes*. ChemBioChem 15, 533–536.

Jirošová, A., Jančařík, A., Menezes, R.C., Bazalová, O., Dolejšová, K., Vogel, H., Jedlička, P., Buček, A., Brabcová, J., Majer, P., Hanus, R., Svatoš, A., 2017. Metabolomic and Transcriptomic Data on Major Metabolic/Biosynthetic Pathways in Workers and Soldiers of the Termite *Prorhinotermes Simplex* (Isoptera: Rhinotermitidae) and Chemical Synthesis of Intermediates of the Defensive (*E*)-nitropentadec-1-ene Biosynthesis (Data in Brief. Submitted).

Kuldová, J., Hrdý, I., Svatoš, A., 1999. Defense secretion of *Prorhinotermes simplex*: toxicity to insecticide susceptible and resistant house fly. J. Chem. Ecol. 25, 657–662.

Kuwahara, Y., Mori, N., Sakuma, M., Tanabe, T., 2003. (1*Z*)- and (1*E*)-2-Nitroethenylbenzenes, and 2-nitroethylbenzene as natural products in defense secretions of a millipede *Thelodesmus armatus* Miyosi (Polydesmida: Pyrgodesmidae). Jpn. J. Environ. Entomol. Zool. 14, 149–215.

Li, T.F., Huo, L., Pulley, C., Liu, A.M., 2012. Decarboxylation mechanisms in biological system. Bioorg. Chem. 43, 2–14.

Meinwald, J., Smolanoff, J., McPhail, A.T., Miller, R.W., Eisner, T., Hicks, K., 1975. Nitropolyzonamine: a spirocyclic nitro compound from defensive glands of a milliped (*Polyzonium rosalbum*). Tetrahedron Lett. 16, 2367–2370.

Merrill Jr., A.H., 2011. Sphingolipid and glycosphingolipid metabolic pathways in the era of sphingolipidomics. Chem. Rev. 111, 6387–6422.

Parry, R., Nishino, S., Spain, J., 2011. Naturally-occurring nitro compounds. Nat. Prod. Rep. 28, 152–167.

Pfaffl, M.W., 2001. A new mathematical model for relative quantification in real-time RT-PCR. Nucleic Acids Res. 29, e45.

Piskorski, R., Hanus, R., Vašíčková, S., Cvačka, J., Šobotník, J., Svatoš, A., Valterová, I., 2007. Nitroalkenes and sesquiterpene hydrocarbons from the frontal gland of three *Prorhinotermes* termite species. J. Chem. Ecol. 33, 1787–1794.

Prestwich, G.D., 1984. Defense mechanisms of termites. Annu. Rev. Entomol. 29, 201–232.

Pruett, S.T., Bushnev, A., Hagedorn, K., Adiga, M., Haynes, C.A., Sullards, M.C., Liotta, D.C., Merrill Jr., A.H., 2008. Thematic review series: sphingolipids. Biodiversity of sphingoid bases ("sphingosines") and related amino alcohols. J. Lipid Res. 49, 1621–1639.

Smith, C.A., Want, E.J., O'Maille, G., Abagyan, R., Siuzdak, G., 2006. XCMS: processing mass spectrometry data for metabolite profiling using nonlinear peak alignment, matching, and identification. Anal. Chem. 78, 779–787.

Šobotník, J., Jirošová, A., Hanus, R., 2010. Chemical warfare in termites. J. Insect Physiol. 56, 1012–1021.

Šobotník, J., Weyda, F., Hanus, R., Cvačka, J., Nebesářová, J., 2006. Fat body of *Prorhinotermes simplex* (Isoptera : Rhinotermitidae): ultrastructure, inter-caste differences and lipid composition. Micron 37, 648–656.

Sonenshine, D.E., 2006. Tick pheromones and their use in tick control. Annu. Rev. Entomol. 51, 557–580.

Spanton, S.G., Prestwich, G.D., 1981. Chemical self-defense by termite workers: prevention of autotoxication in two rhinotermitids. Science 214, 1363–1365.

Spanton, S.G., Prestwich, G.D., 1982. Chemical defense and self-defense: biochemical transformations of contact insecticides produced by soldier termites. Tetrahedron 38, 1921–1930.

Tian, L., Zhou, X.G., 2014. The soldiers in societies: defense, regulation, and evolution. Int. J. Biol. Sci. 10, 296–308.

Vogel, H., Badapanda, C., Knorr, E., Vilcinskas, A., 2014. RNA-sequencing analysis reveals abundant developmental stage-specific and immunity-related genes in the pollen beetle *Meligethes aeneus*. Insect Mol. Biol. 23, 98–112.

Vrkoč, J., Ubik, K., 1974. 1-Nitro-trans-1-pentadecene as defensive compound of termites. Tetrahedron Lett. 15, 1463–1464.

Xia, J., Sinelnikov, I.V., Han, B., Wishart, D.S., 2015. MetaboAnalyst 3.0—making metabolomics more meaningful. Nucl. Acids Res 43, W251–W257.